UC Irvine
UC Irvine Previously Published Works

Title
Larsen B Ice Shelf rheology preceding its disintegration inferred by a control method

Permalink
https://escholarship.org/uc/item/1690f80c

Journal
Geophysical Research Letters, 34(19)

ISSN
0094-8276

Authors
Khazendar, A
Rignot, E
Larour, E

Publication Date
2007

DOI
10.1029/2007gl030980

Copyright Information
This work is made available under the terms of a Creative Commons Attribution License, availalbe at https://creativecommons.org/licenses/by/4.0/

Peer reviewed

eScholarship.org Powered by the California Digital Library
University of California

Larsen B Ice Shelf rheology preceding its disintegration inferred by a control method

A. Khazendar,[1] E. Rignot,[1] and E. Larour[1]

Received 12 June 2007; revised 21 August 2007; accepted 5 September 2007; published 4 October 2007.

[1] A new, complete velocity field from satellite remote sensing is combined with numerical modeling to infer the rheology of the Larsen B Ice Shelf before its disintegration. The resulting spatial distribution of the flow parameter exhibits large variability, which reflects very well observed ice shelf features. This variability is explained by factors including advection of colder ice from tributary glaciers, bottom melting, and the presence of zones of strong shear and fracture. The inferred distribution is applied to simulate numerically the flow regime of the ice shelf and to examine its modification by the presence of open rifts and by the retreat of ice shelf front between 1996 and 2000. Results demonstrate that variable rheology is essential to understanding ice shelf evolution, especially the close relationship among frontal retreat, fracture, ice flow acceleration, and the destabilization of ice shelves. **Citation:** Khazendar, A., E. Rignot, and E. Larour (2007), Larsen B Ice Shelf rheology preceding its disintegration inferred by a control method, *Geophys. Res. Lett.*, *34*, L19503, doi:10.1029/2007GL030980.

1. Introduction

[2] The rapid disintegration of the Larsen B Ice Shelf in 2002 has been attributed to enhanced fragmentation due to increasingly abundant surface meltwater deepening pre-existing crevasses [*Rott et al.*, 1996; *Scambos et al.*, 2000] in an ice shelf made vulnerable by progressive thinning [*Shepherd et al.*, 2003]. Authors have also noted the role of certain areas of weakness in the ice shelf [*Rack et al.*, 2000; *Sandhäger et al.*, 2005; *Vieli et al.*, 2006]. The disintegration, and the progressive two-decade retreat leading to it, have been the subject of modeling studies seeking insight into this example of the destabilization and demise of an Antarctic ice shelf in a warming climate [*Doake et al.*, 1998; *Scambos et al.*, 2000; *Rack et al.*, 2000; *Sandhäger et al.*, 2005]. Such modeling requires the constraining of the proportionality coefficient between stress and strain in Glen's flow law, parameter B, which depends mainly on ice temperature, fabric, impurity and water content [*Paterson*, 1994]. In the absence of adequate theoretical formulations or sufficiently detailed field measurements, modelers of the Larsen Ice Shelf have hitherto either assumed uniform ice stiffness over the entire shelf domain with softening near the margins or calculated the flow parameter from a temperature distribution.

[3] In this work, we combine satellite radar interferometry (InSAR) velocity observations obtained in 2000 with a finite element model of ice shelf flow to infer a spatial distribution of the depth-averaged flow parameter for the whole of Larsen B before its disintegration (Figure 1a) by a control method. Data assimilation on ice shelf rheology has been previously applied to estimate the viscosity of the Ross Ice Shelf [*Rommelaere and MacAyeal*, 1997], the flow parameter of the Ronne Ice Shelf [*Larour et al.*, 2005], and that of Larsen B itself [*Vieli et al.*, 2006]. The latter authors, using a finite difference flow model to invert simultaneously for the flow parameter and boundary velocities, demonstrated the importance of weak zones, but their model did not constrain the rheology of the bulk of the ice shelf.

[4] We explore the different factors that led to the inferred pronounced variability in ice stiffness. We test the ability of this variable rheology to reproduce the flow pattern and magnitudes of the ice shelf and to predict changes in its flow regime following ice shelf front retreat prior to collapse [*Rignot et al.*, 2004]. We further examine the imprint of fracture and weak ice zones on the inferred rheology and their effect on the flow.

2. Input Observations and Model

[5] The ice shelf velocity field (Figures 1b and 1c) was mapped by SAR interferometry to a precision of 5 to 10 m a^{-1} from Radarsat-1 tracks, analyzed with a speckle tracking technique over 24-day time periods starting on September 10, 2000. Ice shelf elevations were taken from the RAMP Antarctic digital elevation model [*Liu et al.*, 1999]. Elevations are less reliable near the grounding line where the source data is older. Ice shelf thickness was calculated from elevation, assuming hydrostatic equilibrium. Velocity and elevation were sampled at 350 m intervals. The grounding line was determined by applying differential pair interferometry to ERS-1/2 measurements from March 1996.

[6] The inversion process seeks a depth-averaged spatial distribution of B that, when substituted into a finite element forward model, minimizes the difference between model output and observations. We use the *MacAyeal* [1989] ice shelf flow model, with InSAR velocity observations imposed at the grounding line. The inverse control method is based on *MacAyeal*'s [1992], except that the boundary condition specified at the ice front is sea water pressure rather than ice velocity; and the flow parameter is directly calculated rather than derived through viscosity, therefore avoiding interpretation difficulties related to viscosity being also a function of the effective strain rate [*Larour et al.*, 2004, 2005]. The model is initiated with an approximate, uniform value of the stiffness, B_0, producing a first estimate of the misfit among modeled and observed velocities. The process is repeated with modified B values until misfit variation falls below 1%.

[1]Jet Propulsion Laboratory, Pasadena, California, USA.

Copyright 2007 by the American Geophysical Union.
0094-8276/07/2007GL030980

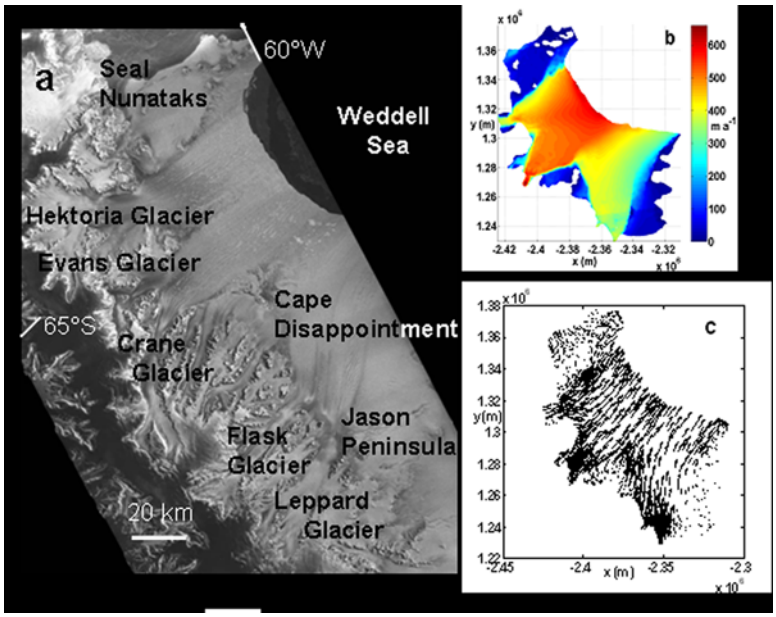

Figure 1. (a) Backscatter image of Larsen B. (b) The speed and (c) vector field of Larsen B as measured in September/October 2000 by Radarsat-1 InSAR.

[7] Observations and model results are shown in polar stereographic coordinates. Our mesh contains 16,000 elements, with element sizes varying between 350 and 2000 m for enhanced representation of ice shelf geometry and features.

3. Results

[8] The model was tested with several initial values at steps of 0.1×10^8 Pa $s^{1/3}$ and found to converge reasonably well in the range from 0.7×10^8 to 1.1×10^8 Pa $s^{1/3}$ (222 to 348 kPa $a^{1/3}$; Figure 2, insets). The experiment output at the middle of the range (Figure 2), with $B_0 = 0.9 \times 10^8$ Pa $s^{1/3}$ (285 kPa $a^{1/3}$), at 60 iterations, is chosen for the analyses below.

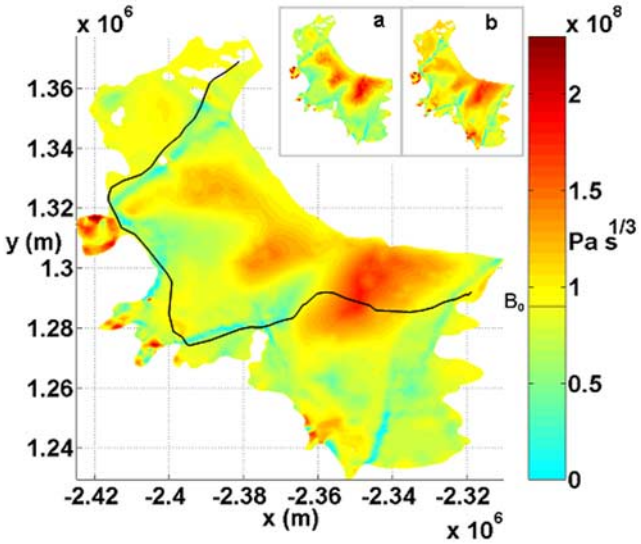

Figure 2. The inferred flow parameter distribution for $B_0 = 0.9 \times 10^8$ Pa $s^{1/3}$. Insets show output at the (a) lower ($B_0 = 0.7 \times 10^8$ Pa $s^{1/3}$) and (b) higher ($B_0 = 1.1 \times 10^8$ Pa $s^{1/3}$) ends of the convergence range. The black line represents the 2002 disintegration front based on an August 24, 2003 MODIS image (from NSIDC).

[9] The most salient aspect of the flow parameter's spatial distribution (Figure 2) is its large variability. Comparing this distribution with features in the backscatter radar image (Figure 1a), it is possible to discern three main areas of stiffer ice that reflect accurately the outflow of colder ice streams. The area furthest north parallels the inflow of the Hektoria, Evans, and Green Glaciers, the central one that of the Crane Glacier, and the southern, the most extensive and stiffest, the Flask and Leppard glaciers. Inferred values for stiffer ice vary from 1.0×10^8 Pa $s^{1/3}$ in the north to 1.9×10^8 Pa $s^{1/3}$ in the south (317 and 601 kPa $a^{1/3}$). Areas of low parameter B sharply delimit stiff ice expanses. They correspond closely to shear zones and highly rifted and crevassed areas that extend in bands from the grounding line to the front (Figure 1a). Fracture in these weak zones probably originated at the lateral margins of outlet glaciers near the grounding line and subsequently advected downstream [*Scambos et al.*, 2000]. They include the bands south of Seal Nunataks, between Hektoria and Crane glaciers, west and southeast of Cape Disappointment and northeast of it extending into the central part of the ice shelf (a zone which previous studies noted the difficulty of simulating [*Sandhäger et al.*, 2005; *Vieli et al.*, 2006]), and the southeast flank of the outflow of Leppard Glacier (Figure 2). Interestingly, this distribution reveals how closely the line of the 2002 disintegration follows the inferred zones of weakness in the northern half of the ice shelf (Figure 2). In the weak zones, B varies mostly between 0.4×10^8 and 0.8×10^8 Pa $s^{1/3}$ (127 and 253 kPa $a^{1/3}$).

4. Discussion

4.1. Improved Forward Modeling and the Importance of Variable Rheology

[10] Testing for improved numerical modeling of ice shelf flow, the output velocity of the forward model using

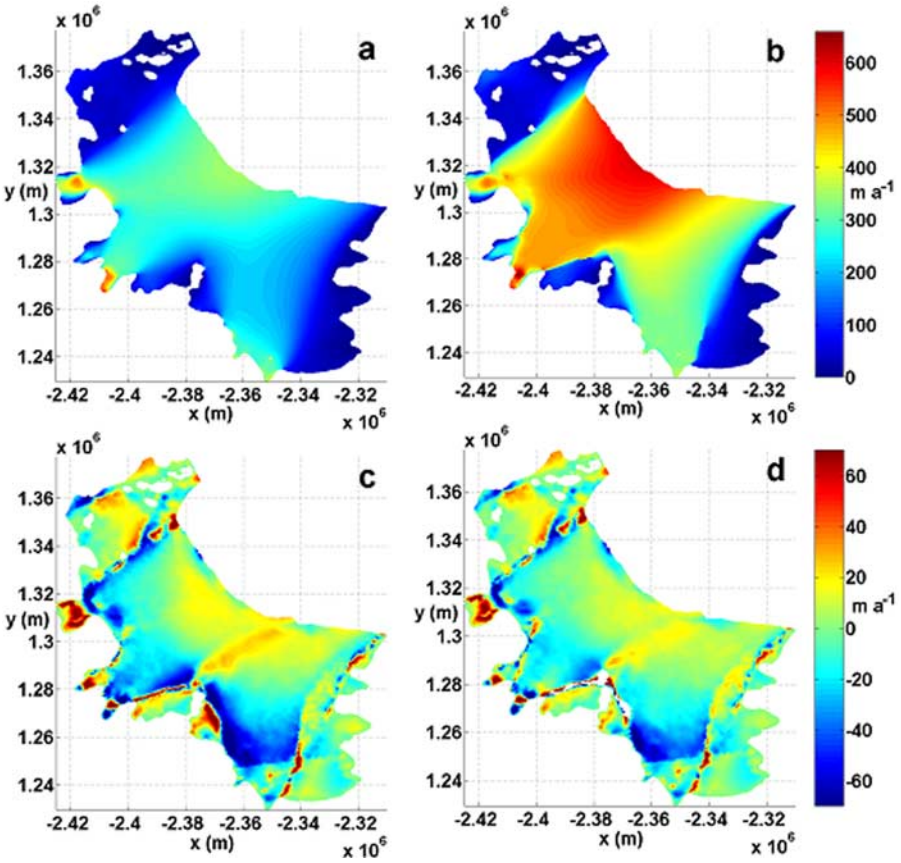

Figure 3. Ice flow speeds for Larsen B simulated by the forward model using (a) a uniform distribution of the flow parameter with B = 1.3 × 10^8 Pa $s^{1/3}$, and (b) the inferred flow parameter distribution from Figure 2. The discrepancy obtained by subtracting the observed speeds from (c) speeds simulated without a rift (Figure 3b), and (d) speeds simulated with a rift included, which appears here as the white area around Cape Disappointment.

our inferred rheology (Figure 2) is compared with that obtained with a uniform, temperature-dependent, value. A representative temperature of −11.0°C, chosen based on *Scambos et al.* [2000], who modeled the temperature distribution of Larsen B using surface and basal temperatures of the ice shelf and those of tributary glacier advections, gives B = 1.3 × 10^8 Pa $s^{1/3}$ (420 kPa $a^{1/3}$) [*Paterson*, 1994]. Running the forward model with this uniform value produces a flow field which compares poorly with observations (Figure 3a). Conversely, the flow field in Figure 3b, generated using our inferred rheology, is in excellent agreement with observations, deviating by less than ±25 m a^{-1} at most locations (Figure 3c), and replicating flow patterns highly accurately, which is a major improvement on earlier attempts [*Vieli et al.*, 2006].

[11] Comparing Figures 3a and 3b shows that using a uniform stiffness results in underestimating not only speeds, but also their spatial gradients everywhere, especially across the weak zones. The large degree of variability in inferred ice rheology clearly functions to concentrate mass flow along certain paths relative to others. This is the main factor in the success of our simulation compared with cases where the domain has uniform stiffness or softened at the margins only.

4.2. Rift Inclusion

[12] Subtracting the observed velocity field (Figure 1b) from that of the reference experiment (Figure 3b) reveals that residual discrepancies occur mostly in and around the strongly fractured and sheared parts of the ice shelf (Figure 3c). Thus, in and downstream from the pronounced fracture zone extending from the northeast of Cape Disappointment toward the front, the model overestimates the speed since it is exaggerating the degree of coupling between the stagnant ice in the fracture zone and the rest of the ice shelf. On the other hand, along the strong shear margins to the west and the southeast of this area, the model tends to underestimate speeds as ice in the model is too strongly coupled with the margins relative to observations. We therefore introduced an open rift around Cape Disappointment, drawing its outline from the radar imagery and constraining it in the finite element mesh domain (Figure 3d) as a dynamic boundary (ice shelf front), i.e., a rift filled with sea water instead of an ice mélange [*Larour et al.*, 2004].

[13] Figure 3d shows that the inclusion of the rift improves significantly the fit between observed and modeled velocities, with flow speeds lower northeast of Cape Disappointment and higher along most shear zones. The improvement affects the entire ice shelf, not only where fracture was introduced.

4.3. Simulating the Observed Shelf Flow Acceleration, 1996–2000

[14] An important aspect of the evolution of Larsen B in the years leading to disintegration is its flow acceleration

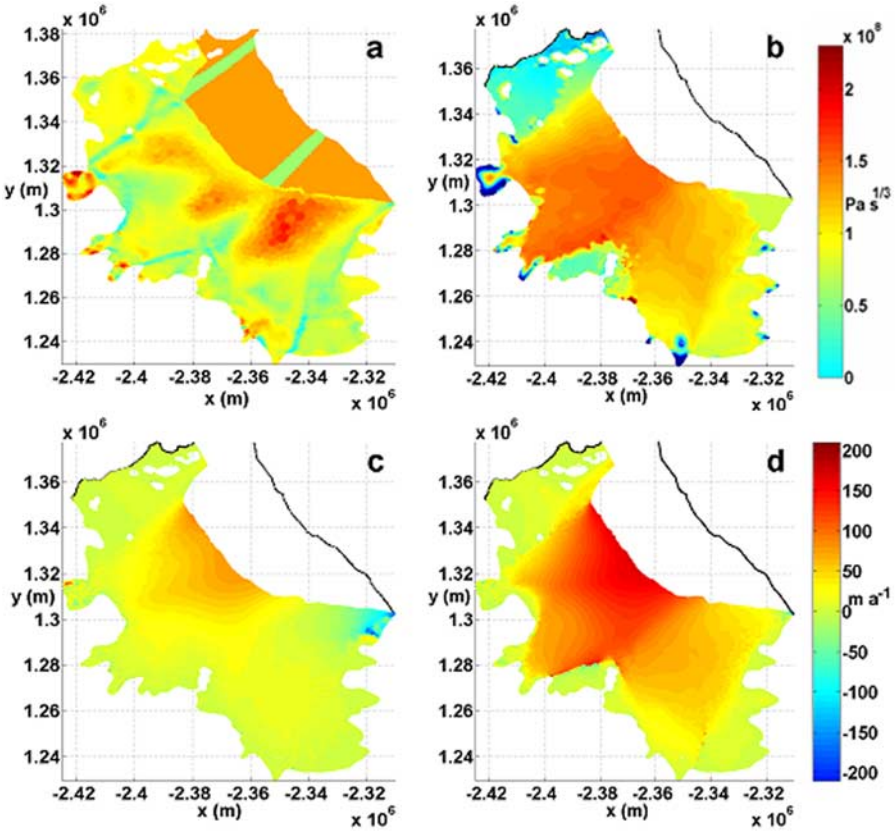

Figure 4. (a) Rheology for the 1996 Larsen B used in simulating flow acceleration between 1996 and 2000 (scale is at top right). The change in ice speed (scale is at bottom right) after front retreat between 1996 (shelf front then is represented by the black dotted line) and 2000 as (b) detected by interferometric analysis of ERS-1/2 observations, (c) modeled with uniform rheology, and (d) modeled with the rheology of Figure 4a.

after large calving events. Flow speed increased by 10% after the calving of 1995 [*Rack and Rott*, 2004] and by 20% after front retreats between 1996 and 2000 [*Rignot et al.*, 2004]. We simulate here the latter event. Since only the change in speed between 1996 and 2000 along a single satellite look-direction, but which coincides with the main direction of flow (given the absence of visible major changes in flow line orientations in the imagery), and not the complete 1996 velocity field, was available, we composed the 1996 ice shelf rheology from the inferred 2000 rheology (Figure 2), plus a simple rheology distribution for the missing part (Figure 4a) consisting of the same uniform value as above $B = 1.3 \times 10^8$ Pa $s^{1/3}$ (420 kPa $a^{1/3}$) intercepted by two weak bands traced along shear zones identified in the 1996 imagery, having $B = 0.6 \times 10^8$ Pa $s^{1/3}$ (190 kPa $a^{1/3}$), which is the value at the middle of the inferred weak area range. We then ran the forward model and compared the calculated velocities with the 2000 velocities. The experiment was repeated for both years with a uniform $B = 1.3 \times 10^8$ Pa $s^{1/3}$ (420 kPa $a^{1/3}$). Compared to observations (Figure 4b), the second experiment predicts little acceleration and does not reproduce the spatial pattern (Figure 4c). The variable B experiment, conversely, while somewhat overestimating the acceleration near the front, replicates the observed pattern convincingly, locating the largest acceleration in the northern part of the ice shelf, in particular along the soft ice zone extending from the grounding line northwest of Cape Disappointment to the center of the ice shelf (Figure 4d). Variable rheology is clearly necessary to explain the observed acceleration.

4.4. Interpreting the Variability of the Flow Parameter

[15] Inferred rheology covers a range between 0.4×10^8 and 1.9×10^8 Pa $s^{1/3}$ (127 and 601 kPa $a^{1/3}$). The higher end corresponds to the three main tributary outflows. Apart from the delimiting strong shear zones and the basal layers, these sectors are probably largely isotropic and temperature is the main factor influencing rheology. The thermal regime model of Larsen B [*Scambos et al.*, 2000] gives ice shelf temperatures at mid-depth from −15.0°C near the grounding line to −10.0°C at the front, corresponding to ice stiffness values between 1.2×10^8 and 1.5×10^8 Pa $s^{1/3}$ (380 and 480 kPa $a^{1/3}$) [*Paterson*, 1994]. These values fit the two stiff areas north of Cape Disappointment. To the south, however, our higher inferred stiffness along the Flask and Leppard glaciers would require temperature as low as −21°C. This area coincides closely, in location and extent, with the part of the ice shelf experiencing the highest rate of thinning, which *Shepherd et al.* [2003] ascribe largely to basal melting. Thermodynamic modeling of ice shelf-ocean interactions [*Holland and Jenkins*, 1999] shows that basal melting lowers the vertical temperature profile of the ice

shelf by several degrees, which would be enough to account for the inferred higher stiffness. Lower temperatures in Flask and Leppard glaciers' outflows could also have resulted from a temporal signature effect [*Rommelaere and MacAyeal*, 1997]. Ice discharged by these two glaciers is older, having grounding line speeds of 350 to 380 m a^{-1}, compared with 620 m a^{-1} for Crane Glacier, making most of it, given the distance to the shelf front, date from the cooler, century-long period starting around 1850 detected by analyses of ice cores from the Dyer Plateau [*Thompson et al.*, 1994] on the Peninsula. By comparison, most of the Crane Glacier ice would have been advected during the time of the warming trend starting around 1950. Furthermore, the relatively higher stiffness of ice south of Cape Disappointment could also be due to less widespread fracture compared with ice in the north, where the presence of rifts and crevasses translates into higher strain rates [*Rack et al.*, 2000] and consequently reduces the inferred value of parameter B.

[16] On the lower end of the rheology range, some of the values inferred in zones of weaker ice are below what would be expected for ice at 0°C [*Paterson*, 1994], an occurrence also noted by *Vieli et al.* [2006]. Investigators of ice shelf processes have already drawn attention to ice conditions that would no longer conform to some of the underlying assumptions of Glen's flow law [*Rommelaere and MacAyeal*, 1997; *Scambos et al.*, 2000]. These low stiffness values reflect the fact that ice in the weak zones is not a homogenous, continuous, and isotropic body. The large velocity gradients across these zones indicate that intense shear stress prevails. The consequent heating, fabric realignment, and increased water content reduce ice stiffness [e.g., *Paterson*, 1994]. Furthermore, open rifts can fill with a mélange of ice shelf fragments, sea ice, and tens of meters of marine ice [*Khazendar and Jenkins*, 2003]. Marine ice has distinct crystallographic structure and salinity and impurity contents [e.g., *Khazendar et al.*, 2001], which affect its rheology and its role in ice shelf fracture [*Larour et al.*, 2004].

4.5. Implications for the 2002 Disintegration Event

[17] The rheology spatial distribution obtained here reveals for the first time how closely the disintegration front in 2002 followed zones of weakness (Figure 2). Yet, the results also show that the effects of soft ice areas manifest themselves within the larger context of a highly variable spatial rheology. Thus, simulating the 1996 to 2000 flow evolution not only shows that front calving is a major factor in the subsequent acceleration, but also that this acceleration was not evenly distributed. A variable rheology channeled the acceleration between the weak zone northeast of Cape Disappointment and the stiff ice zone to the north. Ice flow acceleration along the northern flank of this central fracture zone most likely resulted in further softening through the same processes cited above, including enhanced heating, fabric realignment, and fracture. This agrees with the increased rifting observed between 1995 and 1999 in the area [*Rack and Rott*, 2004], and supports the conclusion by *Sandhäger et al.* [2005] that acceleration was primarily due to front calving and the deepening of shear zones. There was no accompanying change in the velocity of tributary glaciers during the intervening period [*Rignot et al.*, 2004], which must have resulted in further thinning and destabilization of the ice shelf.

5. Conclusions

[18] This study, in its method and outcome, demonstrates the potential of enhancing the ability to predict large-scale ice sheet evolution by making available better observations and more realistic simulations of ice shelf processes. The main observational contribution of this work is the new, highly detailed velocity map of Larsen B relatively close to the time of its disintegration. Our modeling results illustrate the significant interaction and interdependence among front calving, flow acceleration, variable rheology including fracture zones, and the ultimate destabilization of ice shelves. We showed that our inverse modeling method is an accurate and practical option for constraining rheology for entire ice shelves, especially with the increasing availability of satellite observations. The outcome revealed the large variability of the Larsen B Ice Shelf rheology, including observed zones of weakness, which it successfully detected. Most importantly, our convincing simulation of ice shelf flow, its further improvement by the explicit inclusion of fracture with modified boundary conditions, and its ability to predict flow changes due to front retreat emphasize the necessity of realistic rheology to accurate ice shelf numerical modeling, which is indispensable if the reaction of large Antarctic ice shelves to climate change, and their role affecting grounded ice discharge to the ocean, and hence global sea level, is to be elucidated.

[19] **Acknowledgments.** The first author is a fellow of the NRC/Oak Ridge Associated Universities NASA Postdoctoral Program. This work was performed at the Jet Propulsion Laboratory, California Institute of Technology, under contract with the National Aeronautics and Space Administration, Cryospheric Sciences Program. The helpful comments by two anonymous reviewers were much appreciated.

References

Doake, C. S. M., H. F. J. Corr, H. Rott, P. Skvarça, and N. W. Young (1998), Breakup and conditions for stability of the northern Larsen Ice Shelf, Antarctica, *Nature*, *391*, 778–780.

Holland, D. M., and A. Jenkins (1999), Modeling thermodynamic ice-ocean interactions at the base of an ice shelf, *J. Phys. Oceanogr.*, *29*(8), 1787–1800.

Khazendar, A., and A. Jenkins (2003), A model of marine ice formation within Antarctic ice shelf rifts, *J. Geophys. Res.*, *108*(C7), 3235, doi:10.1029/2002JC001673.

Khazendar, A., J. L. Tison, B. Stenni, M. Dini, and A. Bondesan (2001), Significant marine ice accumulation in the ablation zone beneath an Antarctic ice shelf, *J. Glaciol.*, *47*, 359–368.

Larour, E., E. Rignot, and D. Aubry (2004), Modelling of rift propagation on Ronne Ice Shelf, Antarctica, and sensitivity to climate change, *Geophys. Res. Lett.*, *31*, L16404, doi:10.1029/2004GL020077.

Larour, E., E. Rignot, I. Joughin, and D. Aubry (2005), Rheology of the Ronne Ice Shelf, Antarctica, inferred from satellite radar interferometry data using an inverse control method, *Geophys. Res. Lett.*, *32*, L05503, doi:10.1029/2004GL021693.

Liu, H., K. C. Jezek, and B. Li (1999), Development of an Antarctic digital elevation model by integrating cartographic and remotely sensed data: A geographic information system approach, *J. Geophys. Res.*, *104*(B10), 23,199–23,214.

MacAyeal, D. (1989), Large-scale ice flow over a viscous basal sediment: Theory and application to Ice Stream B, Antarctica, *J. Geophys. Res.*, *94*(B4), 4071–4087.

MacAyeal, D. (1992), The basal stress distribution of Ice Stream E, Antarctica, inferred by control methods, *J. Geophys. Res.*, *97*(B1), 595–603.

Paterson, W. S. B. (1994), *The Physics of Glaciers*, 4th ed., Elsevier, New York.

Rack, W., and H. Rott (2004), Pattern of retreat and disintegration of Larsen B ice shelf, Antarctic Peninsula, *Ann. Glaciol.*, *39*, 505–510.

Rack, W., C. S. M. Doake, H. Rott, A. Siegel, and P. Skvarca (2000), Interferometric analysis of the deformation pattern of the northern Larsen Ice Shelf, Antarctic Peninsula, compared to field measurements and numerical modeling, *Ann. Glaciol.*, *31*, 205–210.

Rignot, E., G. Casassa, P. Gogineni, W. Krabill, A. Rivera, and R. Thomas (2004), Accelerated ice discharge from the Antarctic Peninsula following the collapse of Larsen B ice shelf, *Geophys. Res. Lett.*, *31*, L18401, doi:10.1029/2004GL020697.

Rommelaere, V., and D. MacAyeal (1997), Large-scale rheology of the Ross Ice Shelf, Antarctica, computed by a control method, *Ann. Glaciol.*, *24*, 43–48.

Rott, H., P. Skvarça, and T. Nalger (1996), Rapid collapse of northern Larsen ice shelf, Antarctica, *Science*, *271*, 788–792.

Sandhäger, H., W. Rack, and D. Jansen (2005), Model investigations of Larsen B Ice Shelf dynamics prior to the breakup, *FRISP Rep. 16*, pp. 5–12, Bjerknes Cent. for Clim. Res., Bergen, Norway.

Scambos, T., C. Hulbe, M. Fahnestock, and J. Bohlander (2000), The link between climate warming and break-up of ice shelves in the Antarctic Peninsula, *J. Glaciol.*, *46*, 516–530.

Shepherd, A., D. Wingham, T. Payne, and P. Skvarca (2003), Larsen ice shelf has progressively thinned, *Science*, *302*, 856–859.

Thompson, L. G., D. A. Peel, E. Mosley-Thompson, R. Mulvaney, J. Dai, P. N. Lin, M. E. Davis, and C. F. Raymond (1994), Climate since A. D. 1510 on Dyer Plateau, Antarctic Peninsula: Evidence for recent climate change, *Ann. Glaciol.*, *20*, 420–426.

Vieli, A., A. J. Payne, Z. Du, and A. Shepherd (2006), Numerical modelling and data assimilation of the Larsen B ice shelf, Antarctic Peninsula, *Philos. Trans. R. Soc. Ser. A*, *364*, 1815–1839, doi:10.1098/rsta.2006.1800.

A. Khazendar, E. Larour, and E. Rignot, Jet Propulsion Laboratory, Mail Stop 300-319, 4800 Oak Grove Drive, Pasadena, CA 91109, USA. (ala.khazendar@jpl.nasa.gov)